Contract No:

This document was prepared in conjunction with work accomplished under Contract No. 89303321CEM000080 with the U.S. Department of Energy (DOE) Office of Environmental Management (EM).

Disclaimer:

Determining Migration of Vapor Corrosion Inhibitions Within Sandpad

Pavan K. Shukla, Roderick E. Fuentes, Andrew Nordquist, and Bruce J. Wiersma
Battelle Savannah River Alliance, LLC.
Aiken, South Carolina, 29808
USA

Laurie Perry
15059 Conference Center Drive
Chantilly, Virginia, 20151
USA

ABSTRACT

Vapor Corrosion Inhibitors (VCIs) are increasingly being used as a corrosion control measure for soil-side corrosion of Aboveground Storage Tanks (ASTs). VCIs are primarily applied to the tank bottoms using one of the following two delivery methods: (i) through-the-sandpad, and (ii) through-the-floor. Through-the-sandpad delivery is employed for tanks that are in-service, while through-the-floor delivery is used for out-of-service tanks. Access to the tank bottom is relatively uninhibited for the out-of-service tanks, and therefore, VCIs applied using the through-the-floor delivery method are expected to provide coverage to the entire bottom plate. However, for in-service tanks using the through-the-sandpad delivery method, VCIs are injected through the multiple injection ports that are at discrete locations along the ring-wall (single bottom) or dead-shell (double bottom). After VCIs are injected, it is expected that VCIs would migrate via various mechanisms such as molecular diffusion, volatilization, convection, etc., and provide corrosion mitigation coverage throughout the bottom plate. A Pipeline Research Council International (PRCI) sponsored study was conducted to quantify VCI migration for the through-the-sandpad delivery method. Laboratory-scale experiments were conducted to determine VCI migration; two tubular-shaped sand-filled glass vessels were used. VCIs were injected at one end, and electrical-resistance data pre- and post-VCI injection were collected and analyzed to determine the VCI migration rates. The experimental data and associated analysis showed that VCI migrated fairly quickly from the injection points.

Key words: Vapor Corrosion Inhibitors (VCIs), Aboveground Storage Tank, Soil-Side Corrosion, VCI migration.

INTRODUCTION

Soil-side corrosion of AST bottoms is a primary reason for major maintenance expenditures and tank bottom failures and subsequent replacements. Literature data[1,2,3] and experimental work have shown that soil-side corrosion rates could reach as high as 50-100 mpy, indicating that soil-side corrosion could cause the tank-bottom failure in relative short periods, i.e., less than five years after initial installation or repairs.

In addition, a recent PRCI-sponsored study[4] has shown that cathodic protection (CP) systems' effectiveness could be questionable in up to 40 percent of the tanks. Tank operators have been increasingly using the VCIs to address these issues; VCIs are being used singularly or in combination with CP to mitigate tank bottom corrosion. An industry consortium sponsored a study[5] with objectives that also included determining the migration characteristics of VCIs when applied within AST sand tank pad materials. Other objectives of the study were to evaluate CPs' effectiveness for the tank bottom application, monitoring tank pad corrosivity to predict tank bottom corrosion, and determining VCIs' performance under the extreme conditions such as high levels of chloride or high levels of bacteria.

VCI liquid mixtures are routinely injected and distributed throughout the tank sand pad of in-service ASTs. VCI liquid mixtures are also applied through the floors and onto the tank pad surface during out-of-service tank inspection intervals. The most common ways to introduce VCIs into the tank pad include liquid slurry injection (prepared by mixing potable water with VCI) and dry powder application. Determining VCIs' migration characteristics are particularly important when VCIs are delivered through the ports located at discrete positions around the tank ringwall of single bottom tanks, and around the deadshell of double bottom tanks for the in-service conditions. The ports are 20-60 ft apart, and VCIs are pushed either directly through the port, or through a perforated injection tubes connected to the ports. The injection tubes extend into the sandpads various distances under the tank bottoms. Liquid VCI mixtures are released into the sandpad's interstitial space along the length of each perforated tube. In both scenarios of the through-port delivery, a large plume is generated where VCI is released into the sandpad, followed by the continual VCI molecular migration from the plume mass. VCIs' migration to the tank bottom in the molecular state is accomplished through the process of chemical volatilization and diffusion for distribution of the inhibitor chemistry until equilibrium is achieved. The VCI chemistries then continually emit molecules that collect on the tank bottom in sufficient concentration to mitigate corrosion for extended duration.

EXPERIMENTAL

Two identical experimental units were built. An image of the experimental setup is presented in Figure 1. As seen in the figure, the two units are side-by-side, the front unit is more clearly visible than the one in the back. Location of the VCI injection port, first and second electrical resistance (ER) probes, and Ultrasonic transducer (UT)-based coupon is marked in Figure 1. A schematic of the experimental setup unit is presented in Figure 2. Each experimental unit was assembled using three parts: (i) injection port section, (ii) ER probe section, and (iii) UT probe section. The internal diameter of the ER probe section was 5.5 inch, and so was that of the injection port and UT probe sections near the adjoining areas of the ER probe section. The UT port section was tapered at UT port end to match dimensions of the UT coupon assembly. The three parts of each unit were assembled using the two steel clamps, as seen in Figure 1.

Set-up for each experiment was as follows. A fixed amount of the field sand was measured and portioned for each experiment. Sodium chloride and sodium sulphate salts were added and thoroughly mixed. Sufficient amount of tap water was added to achieve approximately 75 percent water saturation, and the resulting mixture was loaded into in each experimental unit. Five mass-loss coupons were placed during assembling of each unit as shown in Figure 3. ER probes and UT coupons were placed after completing the assembly. The probes and coupons were exposed to the pre-VCI sand condition in each unit for approximately 4.5 months; VCIs were added approximately 4.5 months from after test initiation. Various material amounts used in the two experiments, and start, VCI injection, and end dates of the experiments are provided in the PRCI report. The two experiments were conducted at the laboratory conditions with ambient temperature being approximately 22 °C.

In each experimental unit, the first and second ER probes in each experimental units were approximately 1 and 2 ft from the VCI injection points, respectively, and the mass-loss coupons were placed approximately 3 ft from the injection points.

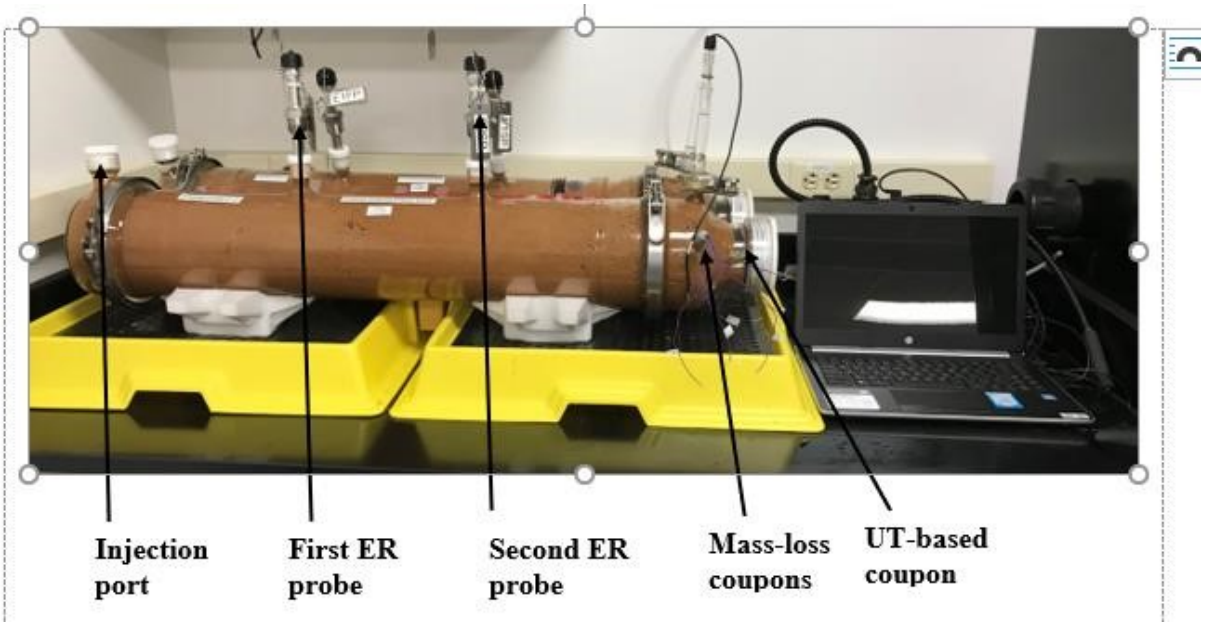

Figure 1: Image of the experimental setup used to study VCI migration.

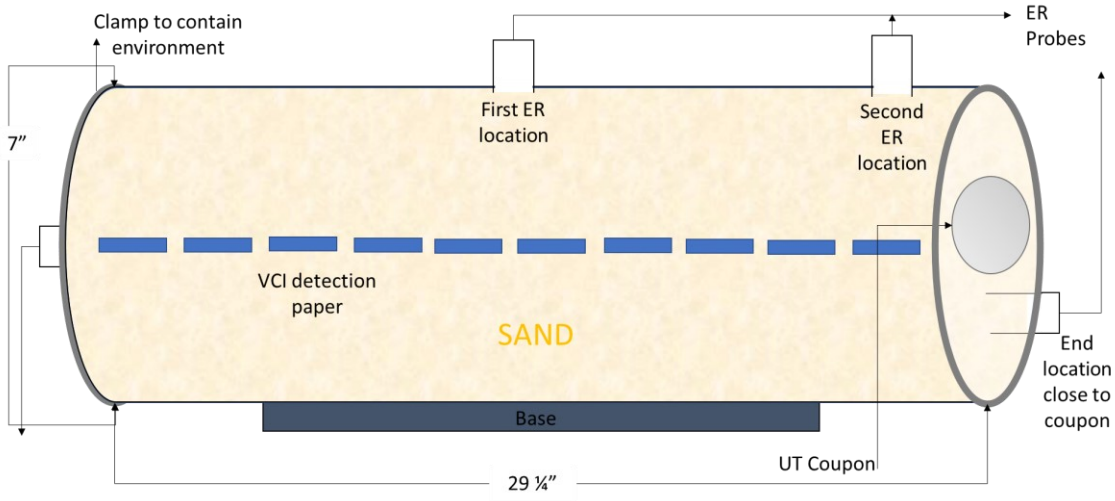

Figure 2: Schematic of a VCI migration setup unit

Figure 3: Image of the mass-loss coupons placed inside migration experimental unit

EXPERIMENTAL DATA AND RESULTS

ER probe data were continually collected. The mass-loss coupons' potentials were recorded, and UT-based mass loss coupons thickness measurements were made. The data from the ER probes and mass-loss coupons are analyzed and associated results are discussed next.

Electrical Resistance Probe Data

ER probe measurements were repeated several times each day; this allowed estimation of ER probe data variance. Experiment 1 data for the first and second ER probes are presented in Figure 4(a) and Figure 4(b), respectively; as seen in the figure, multiple measurements were conducted for a given day, and each set of measurements for a given day differed with each other. The multiple measurements for a given day allowed for estimation of ER probe data variance. The variance estimate is critical to accurately determine the migration rate. It is implicitly assumed that the probes did not significantly corrode during the measurement period, which is approximately 30-40 minutes for approximately twenty measurements using the ER probe data logger. The Experiment 1 ER probe data were processed and average ± standard deviation for the first and second ER probes are presented in Figure 5(a) and Figure 5(b), respectively; as seen in the figures, standard deviations vary with measurements.

Experiment 2 data for the first and second ER probes were also scanned with multiple measurements for a given day, and each set of measurements for a given day differed with each other. The Experiment 2 ER probe data were processed and average ± standard deviation for the first and second ER probes are presented in Figure 6(a) and Figure 6(b), respectively; as seen in the figures, standard deviations vary with measurements. A variance distribution plot of the first and second ER probe data is presented in Figure 6. As seen in the figure, most of the standard deviation range between 0.06 to 0.19 mil, with the mode of 0.13 mil. There are few outliers in terms of variances: two in the first ER probe data, and one in the second ER probe data. The two standard deviation outliers in the first ER probe data are at 0.29 and 0.34 mil, and one in the second ER probe data at 0.25 mil.

The initial and final Experiment 1 first ER probe data values are approximately 1.0 to 2.5 mil for the duration of the migration experiment. Using the variance mode value of 0.13, the least and maximum possible difference between the initial and final ER probe data is 0.88 and 1.92 mil with the 95% probability range; both values are above zero, indicating significant differences in the ER probe data. If the variance of 0.19 mil is used on the first ER probe data, the least and maximum possible difference between the ER probe data is 0.64 and 2.16 mil within the 95% probability range, still both values being above zero. Therefore, the first ER probe data is deemed sufficient to use to estimation the VCI migration effect. The initial and final Experiment 1 second ER probe data values are approximately 1.5 to 2.25 mil for the duration of the migration experiment. Using the variance mode value of 0.13, the least and maximum possible difference between the initial and final ER probe data is 0.23 and 1.27 mil with the 95% probability range. However, if the variance of 0.19 mil is used on the second ER probe data, the least and maximum possible difference between the initial and final ER probe data is -0.01 and 1.51 mil with the 95% probability range. This indicates that the large variance in the data may confound interpretation of the ER probe data for estimating the migration rate. Therefore, the Experiment 1 second ER probe data was not used. The visual examination of the Experiment 1 ER probes indicated that both probes had similar levels of corrosion. Therefore, it is likely that Experiment 1 second ER probe was malfunctioning during the experiment.

Average values of the Experiment 1 First ER probe data are presented in Figure 5(a); the VCI injection occurred on day-139, and it is marked by the solid gray line in the figure. The ER probe data continued to increase even after that and reached a value of 2.47 mil on day-161. The ER data is 2.51 on day-272, i.e., the last day of the experiment. The difference in the day-272 and day-161 values is 0.04 mil, which is less than the least variance value of 0.06 mil in Figure 7(a). The p-value between day-161 day-272 ER probe data is 0.13, indicating that two sets of measurements are statistically similar. This indicated

that it took approximately 3 weeks for the VCI-B to be effective in mitigating corrosion on the Experiment 1 first ER probe.

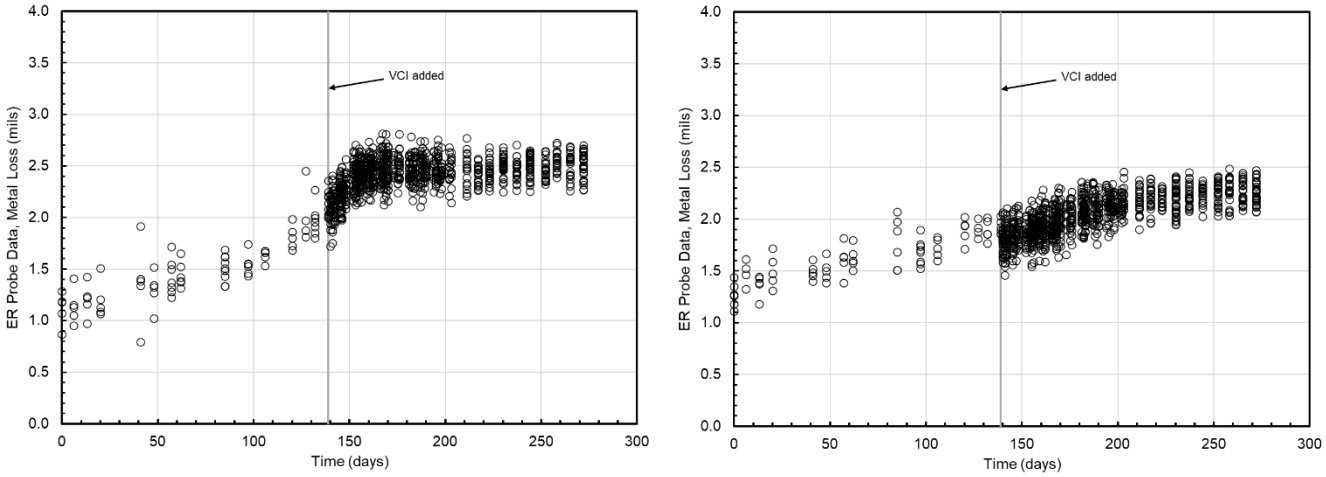

(a) Experiment 1 First ER Probe data **(b) Experiment 1 Second ER Probe data**

Figure 4: Experiment 1 (a) First ER probe and (b) Second ER probe data

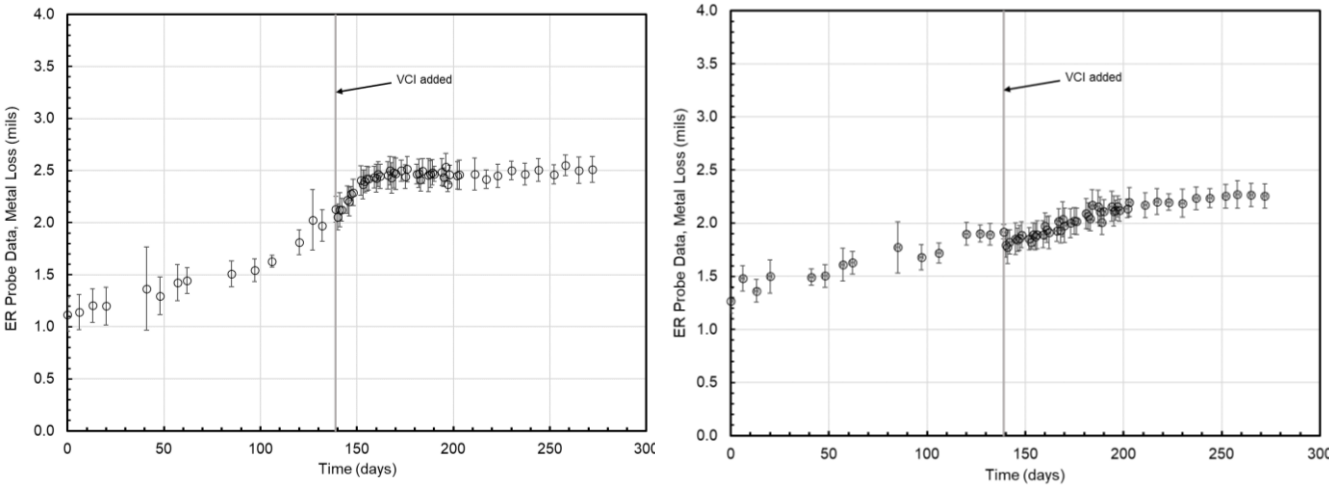

(a) Experiment 1 First ER Probe data **(b) Experiment 1 Second ER Probe data**

Figure 5: Experiment 1 (a) First ER probe and (b) Second ER probe data with average and standard deviation for each data point. The standard deviations are represented by the black vertical line for each data point.

The Experiment 2 First ER probe data are analyzed; the ER probe data average values are presented Figure 8(a). The pre-VCI data in Figure 8(a) are represented by orange symbols. A liner fit of the pre-VCI data was obtained and is represented by the dash-line in Figure 8(a). The linear fit is extrapolated after VCI injection, and extrapolation is represented by the solid black line in the figure; the First ER probe data immediately after VCI injection falls below the extrapolated line, showing that the VCI was immediately effective after injection. The Student's t-test was applied to determine the point of inflection and the transient region. Day-271 ER probe data was statistically compared to the previous data points, and when p-value was below 0.05, that data was the inflection point. The p-value between the Day-271 and Day-169 was 0.08 and between Day-271 and Day-167 was 0.01. The p-values between the Day-271 and any data point before Day-167 were less than 0.05. Considering the p-values, Day-169 ER probe data was established as the inflection point. The VCI injection occurred on Day-138, thus it took

approximately 30 days to VCI completely mitigate the ER probe material corrosion. The data region between Day-138 and Day-167 is highlighted by a light-blue rectangle. This region is de-fined as transient region post-VCI injection. The corrosion rate pre-VCI injection was 5.9 mpy, and 0.95 mpy in the transient region, indicating that injected VCI was effective in mitigating during the transient period.

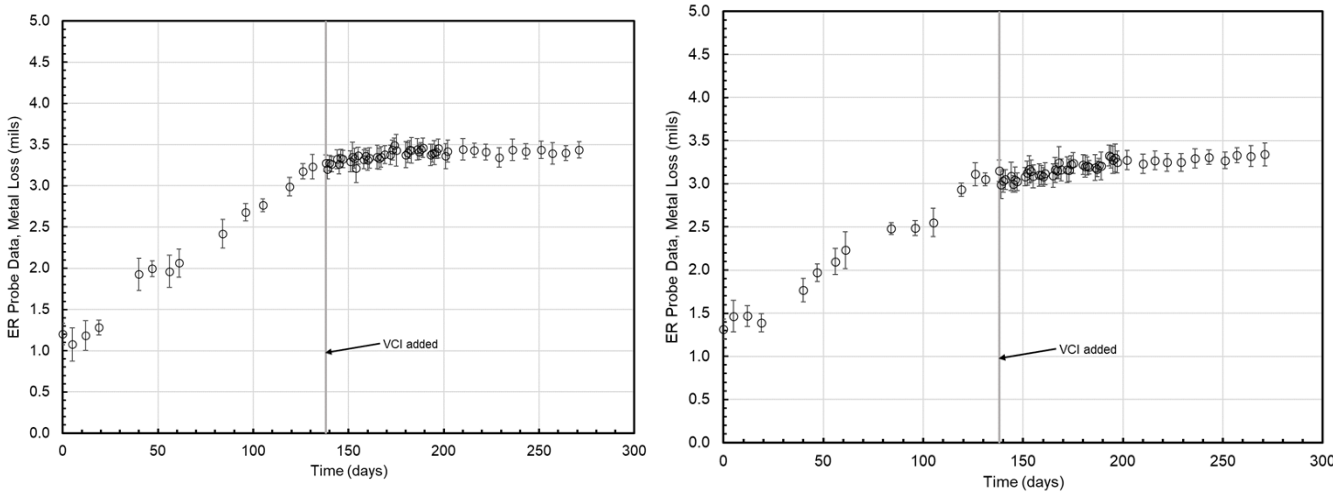

(c) Experiment 2 First ER Probe data **(d) Experiment 2 Second ER Probe data**

Figure 6: Experiment 2 (a) First ER probe and (b) Second ER probe data with average and standard deviation for each data point. The standard deviations are represented by the black vertical line for each data point.

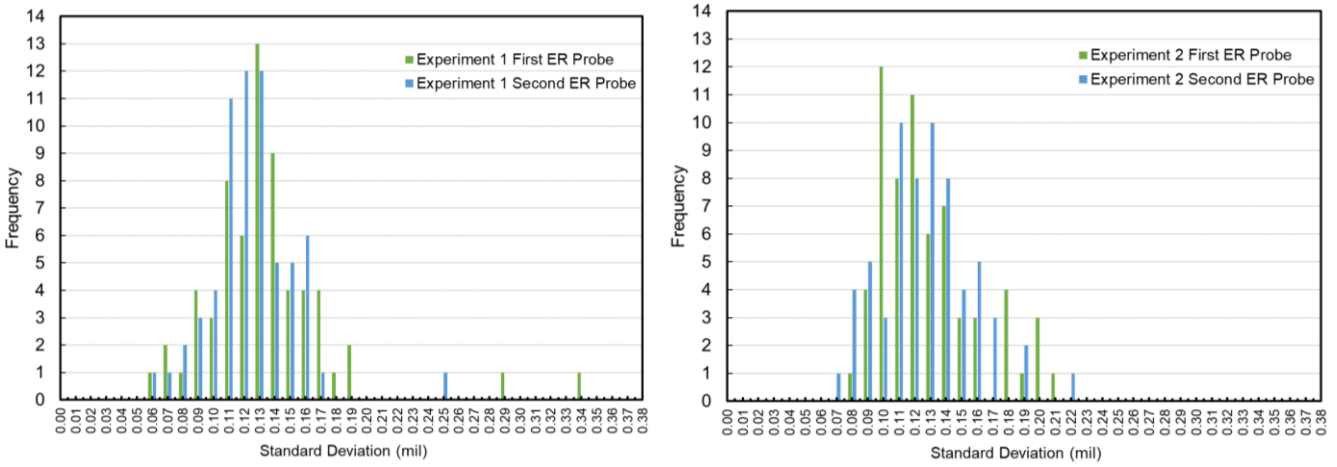

(a) Experiment 1 **(b) Experiment 2**

Figure 7: Variance distribution plots for the (a) Experiment 1 and (b) Experiment 2 First and Second ER probe data

The Experiment 2 Second ER probe data is analyzed in similar fashion as the First ER probe data. The average values of the ER probe data are presented Figure 8(b) where pre-VCI data is represented by orange symbols. A linear fit of the pre-VCI injection data was obtained and is represented by the dash-line in Figure 8(b). The linear fit is extrapolated after VCI injection, and extrapolation is represented by the solid black line in the figure; the Second ER probe data and VCI injection falls below the extrapolated line, showing that the VCI was immediately effective after injection. The Student's t-test was applied to determine the point of inflection and the transient region. The p-value between the Day-271 and Day-193 was 0.74 and be-tween Day-271 and Day-189 was 0.006. The p-values between the Day-271 and

any data point before Day-189 were less than 0.05. Considering the p-values, Day-193 ER probe data was established as the inflection point. The VCI injection occurred on Day-138, thus it took approximately 55 days to VCI completely mitigate the ER probe material corrosion. The data region between Day-138 and Day-193 is highlighted by a light-blue rectangle. This region is defined as transient region post-VCI injection for the Experiment 2 Second ER probe. The corrosion rate pre-VCI injection was 4.9 mpy, and 1.16 mpy in the transient region, showing that the injected VCI was effective in mitigating corrosion even during the transient period.

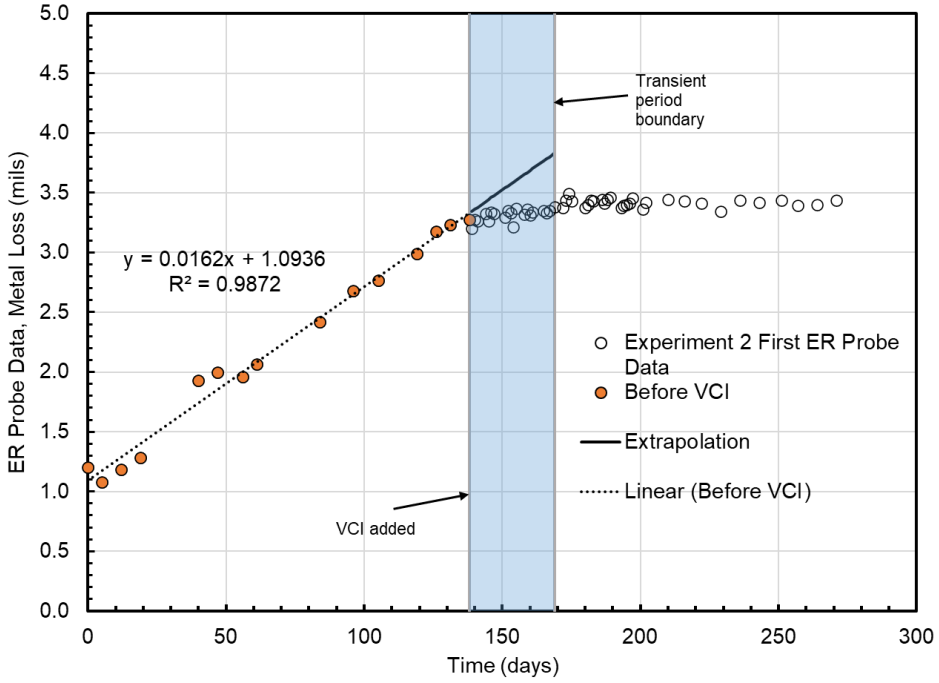

(a) **Experiment 2 First ER Probe**

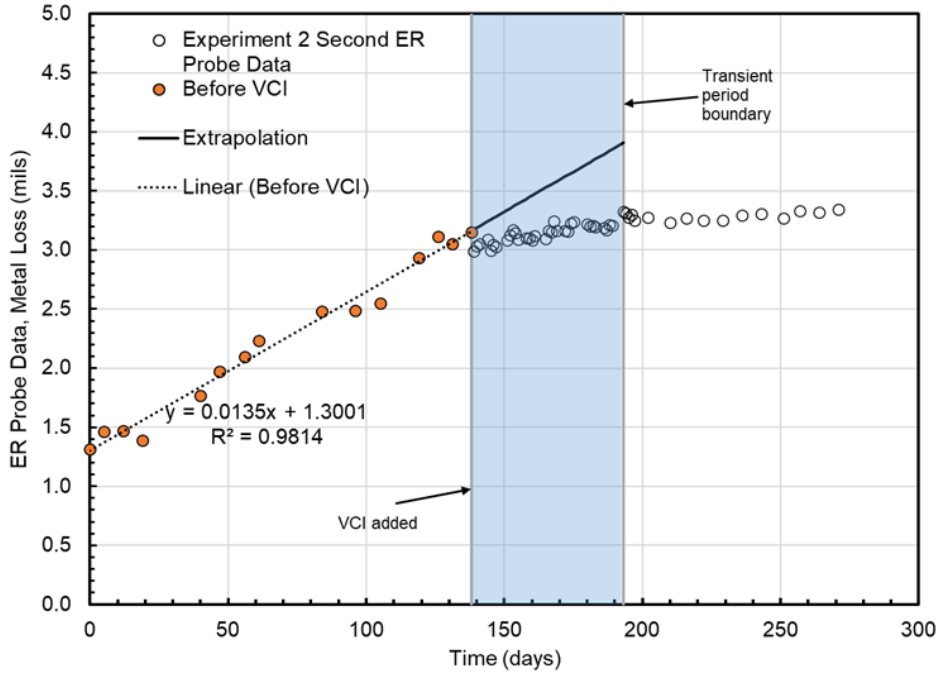

(b) Experiment 2 Second ER Probe

Figure 8: Experiment 2 (a) First ER probe and (b) Second ER probe data with average values. The transient regions after VCI addition are highlighted by the light-blue rectangles.

The analyzed data for Experiment 1 and Experiment 2 ER probes are summarized in Table 1.

Table 1. Summary of Electrical Resistance Probe Data Analysis

Experiment	ER Probe	Pre-VCI Corrosion Rate (mpy)	Transient Period Duration (days)	Transient Period Corrosion Rate (days)	Post Transient Period Corrosion Rate** (mpy)
Experimental Unit 1	First ER Probe (~ 1 ft from injection)	5.08	22	5.62	0.14
	Second ER Probe* (~ 2 ft from injection)	–	–	–	–
Experimental Unit 2	First ER Probe (~ 1 ft from injection)	5.91	31	0.95	0.21
	Second ER Probe (~ 2 ft from injection)	4.93	55	1.16	0.07

*Experiment 1 Second ER probe data was not sufficient to make statistically significant distinctions between pre- and post-VCI periods. Therefore, the ER probe data were not used.
**Post-transient period corrosion rates are calculated using the ER probe metal loss averages.

Coupon Corrosion Potential Data

The Phase 1 PRCI study[5] on the VCIs' application for AST bottoms indicated that corrosion potentials could be used to distinguish between presence and absence of the VCIs. Five mass-loss coupons were placed as sketched in Figure 3. An image of the coupons placed in one of the experiments is shown in Figure 3. The coupons are labeled in numerical order. The coupons in Experiment 1 are labeled as Coupons 1-5, and in Experiment 2 as Coupons 6-10. The corrosion potential data of the coupons in Experiment 1 is presented in Figure 9(a) and for Experiment 2 in Figure 9(b); the VCI addition day is marked by the vertical dashed lines in the two figures.

The x-axis range was changed to enhance view of the data before and after VCI. Experiments 1 and 2 coupons' corrosion potentials during day-120 to day-190 is presented in Figure 10(a) and 10(b), respectively. In Experiment 1, corrosion potentials of Coupons 1 and 2 ranged between -600 to -650 mV with respect to saturated calomel electrode (SCE), and corrosion potentials of Coupons 3, 4, and 5 were in the range of -750 to -800 mV_{SCE}. Corrosion potentials of the Coupons 1 and 2 became more cathodic immediately after VCI addition, whereas corrosion potentials of the Coupons 3, 4, and 5 continued to be in the range of -750 to -800 mV_{SCE} even after VCI addition. Corrosion potential of Coupon 1 reached the most cathodic value of -668 mV_{SCE} on day-153, whereas corrosion potential of Coupon 2 reached the most cathodic value of -724 mV_{SCE} on day-168. The coupons were acid cleaned post-completion of the

experiments. The Experiment 1 coupons' surface average and deepest pit corrosion rates are listed in Table 2. The surface average corrosion rates of Coupons 1 and 2 are 1.61 and 1.18 mpy, respectively, whereas corrosion rate calculated form the Experiment 1 First ER probe data is 1.83 mpy. The corrosion rate data of Coupons 1 and 2 are fairly close to that of the ER probe derived corrosion rates.

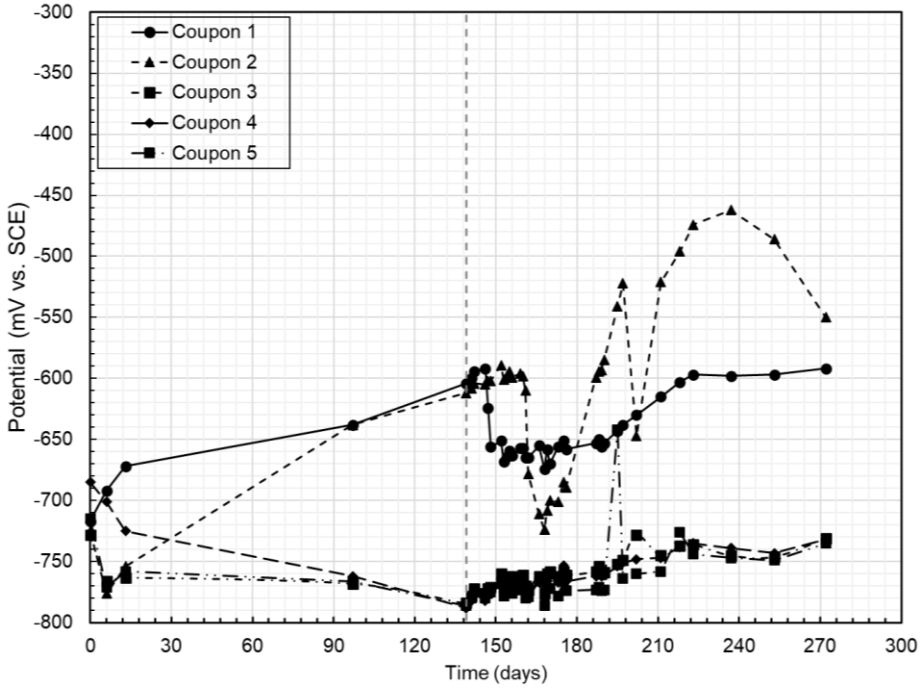

(a) Experiment 1 Coupon Corrosion Potential

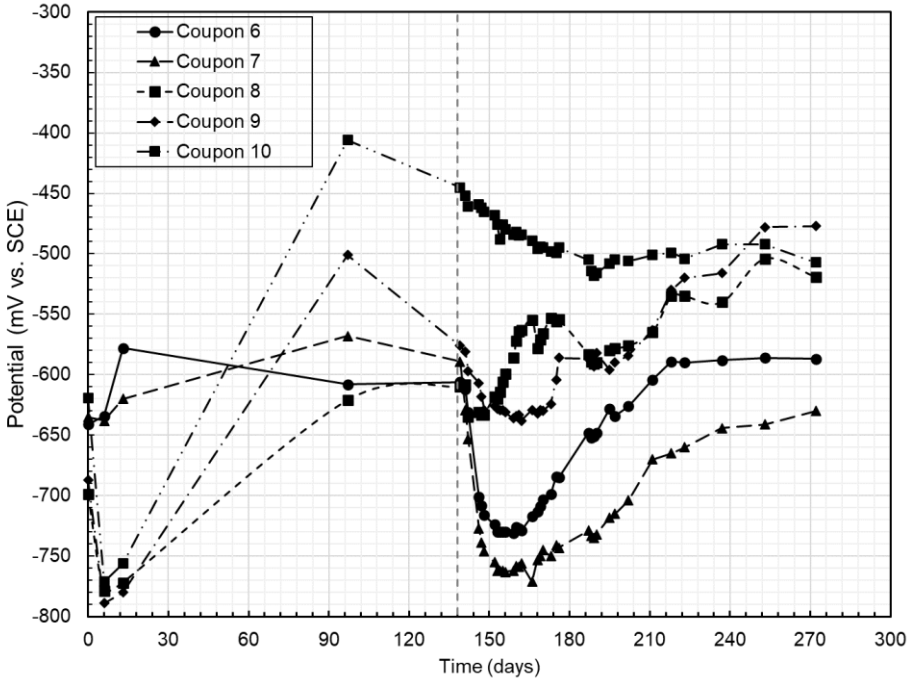

(b) Experiment 2 Coupon Corrosion Potential

Figure 9: Corrosion potential data of the mass-loss coupons in the migration (a) Experiment 1 and (b) Experiment 2. The VCI addition day is marked by the vertical dash line.

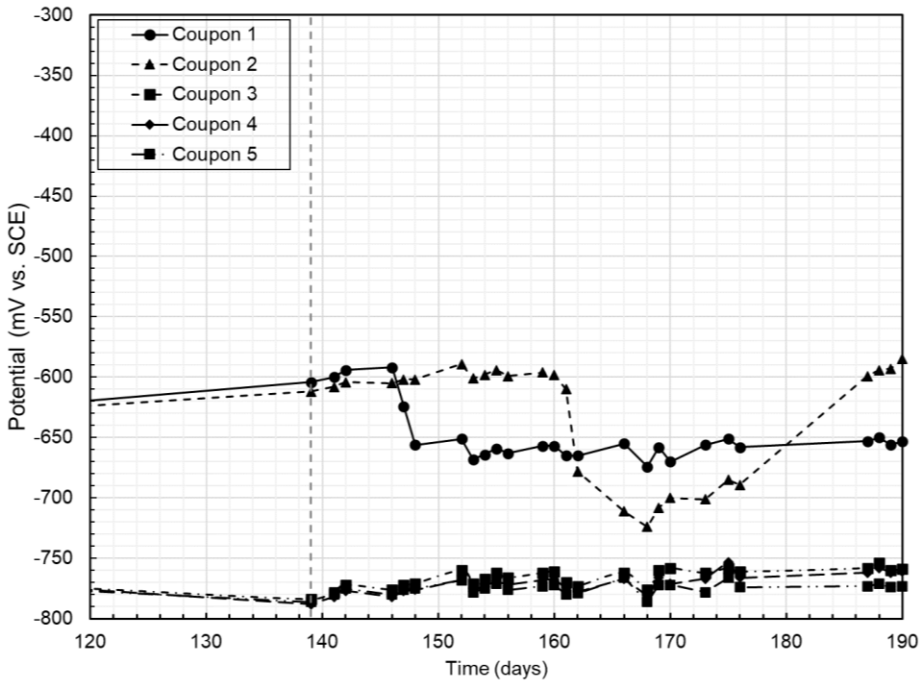

(a) Experiment 1 Coupon Corrosion Potential

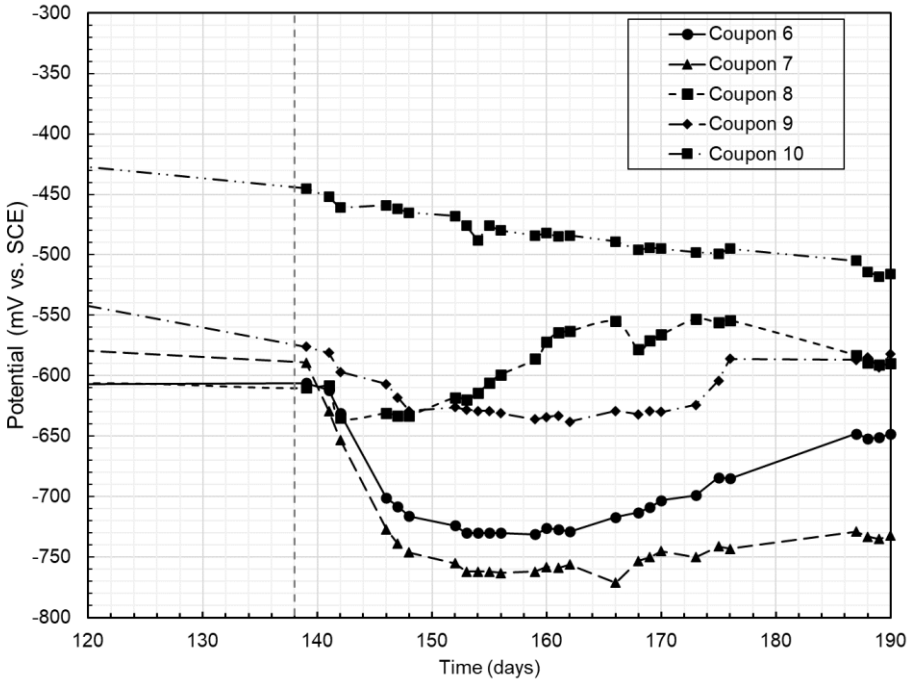

(b) Experiment 2 Coupon Corrosion Potential

Figure 10: Mass-loss coupons corrosion potentials during day-120 and day-190 in the migration (a) Experiment 1 and (b) Experiment 2. The VCI addition day is marked by the vertical dash line.

The corrosion potentials of the Coupons 3-5 in Experiment 1 did not change after VCI injection. In addition, the surface average corrosion rates of the Coupons 3-5 are much lower than Coupons 1 and 2. It is possible that Coupons 3-5 were not in complete contact with the sand electrolyte. The coupons faces were vertical with respect to the ground surface. As a result, the sand electrolyte may have slightly shifted during the setup., disturbing close contact between Coupons 3-5 and sand electrolyte.

Experiment 2 coupons corrosion potentials during day-120 to day-190 is presented in Figure 10(b). The corrosion potentials of Coupons 6 and 7 were approximately -610 mV_{SCE} and -590 mV_{SCE}, before VCI injection.; the coupons' corrosion potentials started to become more cathodic immediately after injection. The corrosion potential of Coupon 6 reached the most cathodic value of -730 mV_{SCE} on day-156, whereas the corrosion potential of Coupon 7 reached the most cathodic value of -756 mV_{SCE} on day-156. The corrosion potentials of Coupons 8-10 also became more cathodic after VCI injection, but the trends were not as smooth as that for Coupons 6 and 7. Therefore, Coupons 8-10 corrosion potential data were not considered to be reliable indicators of the VCI migration. Coupons 6-10 were acid cleaned post-experiment. The Experiment 2 coupons' surface average and deepest pit corrosion rates are listed in Table 2. The surface average corrosion rates of Coupons 6 and 7 are 3.3 and 2.57 mpy, respectively, whereas corrosion rate calculated form the Experiment 2 First and Second ER probe data are 3.0 and 2.73 mpy. The corrosion rate data of Coupons 6 and 7 are fairly close to that of the Experiment 2 ER probe derived corrosion rates, indicating that both Coupons 6 and 7 and ER probes experienced similar electrolyte environment, even though the mass-loss coupons and ER probes were not co-located. This further indicated that VCIs migration is rapid. In addition, while the corrosion potential is not a very strong indicator of VCI presence, it can be used in field to detect VCI migration.

The corrosion potentials of the Coupons 8-10 in Experiment 2 did change and became cathodic after VCI injection. However, the magnitude of the change was not as much as in Coupons 6 and 7, and the change direction was not as smooth as in the Coupons 6 and 7. Similar to Experiment 1, it is possible that Coupons 8-10 were not in complete contact with the sand electrolyte in Experiment 2. The coupons faces were vertical with respect to the ground surface. As a result, the sand electrolyte may have slightly shifted, and disturbed close contact between the sand and Coupons 8-10 surfaces.

Table 2. Migration Experiment Mass-Loss Coupon Corrosion Rate

Experiment	Coupon	Surface Average Corrosion Rate (mpy)	Deepest Pit Corrosion Rate (mpy)	Consistency with ER Probe Data	Notes
Experiment 1	1	1.61	13.5	First ER probe corrosion rate = 1.83 mpy, Coupons 1 and 2 corrosion rates are consistent with ER probes	Coupons 1 and 2 corrosion potential dipped by -100 and -200 mV, respectively, coupons potentials became more cathodic. The largest dipped occurred approximately 28 days after injection.
	2	1.18	17.9		
	3	0.33	1.3		
	4	0.33	1.1		
	5	0.32	1.5		
Experiment 2	6	3.30	38.0	First and Second ER probe corrosion rates = 3.00 and 2.73 mpy. Coupons 6 and 7 corrosion rates are consistent with ER probes	Coupons 5 and corrosion potential dipped by -130 and -170 mV, respectively. Coupons' potentials became more cathodic. The largest dipped occurred approximately 18 days after injection.
	7	2.57	21.5		
	8	0.84	12.3		
	9	0.58	12.4		
	10	0.48	5.8		

CONCLUSION

The ER probe data clearly indicated the effect of VCI on corrosion. The data also showed that VCIs migrated rapidly through the sand electrolyte. For each ER probe, there was a metal-loss transient period after injection of the VCIs. The transient period ranged from 3-8 weeks. The corrosion potential of the mass-loss coupon data indicated that the corrosion potentials were more cathodic after VCI injection. However, the change in corrosion potentials after VCI injection was not consistent across all the coupons. The migration study showed that ER probes are most consistent in detecting the presence of VCI. This finding is consistent with the previous PRCI study where ER probe and coupons' corrosion rates were within the range of each other.

ACKNOWLEDGEMENTS

The authors acknowledge Pipeline Research Council International, Inc. and its members for funding and in-kind support. The authors also acknowledge the VCI manufactures for providing their products for the study.

This work was produced by Battelle Savannah River Alliance, LLC under Contract No. 89303321CEM000080 with the U.S. Department of Energy. Publisher acknowledges the U.S. Government license to provide public access under the DOE Public Access Plan (http://energy.gov/downloads/doe-public-access-plan)."

REFERENCES

1. E. Lyublinski, G. Ramdas, Y. Vaks, T. Natale, M. Posner, K. Baker, R. Singh, and M. Schultz. "Corrosion Protection of Soil Side Bottoms of Aboveground Storage Tanks." CORROSION/2014, Paper No. 4337 (Houston, TX, NACE, 2014).

2. E. Lyublinski, K. Baker, T. Natale, M. Posner, G. Ramdas, A. Roytman, and Y. Vaks. "Corrosion Protection of Storage Tank Soil Side Bottoms Application Experience." CORROSION/2015, Paper No. 6016 (Houston, TX, NACE, 2015).

3. T. Whited, X. Yu, and R. Tems. "Mitigating Soil-Side Corrosion on Crude Oil Tank Bottoms Using Volatile Corrosion Inhibitors." CORROSION/2013, Paper No. 2242, (Houston, TX, NACE, 2013).

4. P. Shukla, A. Nordquist, R. Fuentes, B. Wiersma, "Vapor Corrosion Inhibitors Effectiveness for Tank Bottom Plate Corrosion Control – Phase 2," Report Catalog Number PR644-183611-R01. (Chantilly, VA: PRCI, Inc. 2022).

5. P. Shukla, X. He, O. Pensado, A. Nordquist, "Vapor Corrosion Inhibitors Effectiveness for Tank Bottom Plate Corrosion Control," Report Catalog Number PR–015–153602-R01. (Chantilly, VA: PRCI, Inc. 2018).